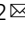


Self-healing liquid metal composite for reconfigurable and recyclable soft electronics

Ravi Tutika ¹, A. B. M. Tahidul Haque ¹ & Michael D. Bartlett ^{1,2} 

Soft electronics and robotics are in increasing demand for diverse applications. However, soft devices typically lack rigid enclosures which can increase their susceptibility to damage and lead to failure and premature disposal. This creates a need for soft and stretchable functional materials with resilient and regenerative properties. Here we show a liquid metal-elastomer-plasticizer composite for soft electronics with robust circuitry that is self-healing, reconfigurable, and ultimately recyclable. This is achieved through an embossing technique for on-demand formation of conductive liquid metal networks which can be reprocessed to rewire or completely recycle the soft electronic composite. These skin-like electronics stretch to 1200% strain with minimal change in electrical resistance, sustain numerous damage events under load without losing electrical conductivity, and are recycled to generate new devices at the end of life. These soft composites with adaptive liquid metal microstructures can find broad use for soft electronics and robotics with improved lifetime and recyclability.

¹Mechanical Engineering, Soft Materials and Structures Lab, Virginia Tech, Blacksburg, VA, USA. ²Macromolecules Innovation Institute, Virginia Tech, Blacksburg, VA, USA. email: mbartlett@vt.edu

Soft electronics are critical components for emerging fields, such as soft robotics, wearable electronics, and human-machine interfaces^{1–3}. In contrast to rigid electronics, which are protected with stiff external supports and enclosures when deployed, soft electronics must maintain extreme compliance and cannot use these traditional means of protection, which can render them vulnerable^{4–6}. Thus, everyday environments can lead to wear, tear, and unexpected damages, which will ultimately result in failure and premature disposal^{7–9}. If sustained damage is severe or a device with another purpose is needed, self-healing no longer provides a significant benefit and regeneration to a pristine state is required. This highlights the need to design the life cycle of soft electronic devices to create tunable systems that can survive in the diverse and emerging application space^{10,11}. Therefore, in addition to being soft, stretchable, and electrically conductive, robust soft electronics can benefit from being self-healing, damage tolerant, reconfigurable, and ultimately recyclable.

A powerful approach to create regenerative electronics is to program in biologically inspired, autonomous functions to protect them from, and to limit, damage, or even to reverse damage and regenerate^{7,12,13}. One example of this method has been to develop transient electronics, which can dissolve at the end of life^{14,15}, and can be made stretchable with geometrically patterned conductors¹⁶. Another avenue to impart stretchability in electronics is to deposit conductive inks onto inherently stretchable textile materials or fiber mats^{17,18}. Rehealable and recyclable electronic skins based on dynamic covalent networks with rigid conductive particles can be created, but healing requires manual intervention and the networks are not stretchable beyond a few percent strain¹⁹. Another approach is to utilize solid-liquid composites, such as liquid metal-based elastomers^{20–26}. Liquid metal-based electronics that have manually repairable or reclaimable properties have been explored, but only show modest stretchability^{27–29}. Liquid metal-elastomer composites have shown autonomous self-healing similar to microcapsuled healing approaches^{30,31}. Key to these materials is the ability to make electrically conductive pathways from discrete liquid metal droplets, which has been shown with scribing/writing or laser sintering^{32,33}. Though these methods have shown promise, electrical resistance typically increases with strain and there is limited or no control on the resistance of a trace. Present methods to make conductive traces in soft composites also create permanent traces or can be reconfigured, but do not fully return to an electrically insulating state to create new electronic circuitry^{30,34}. Thus, materials that can realize robust, highly stretchable conductors with reconfigurability and regeneration at the end of its life cycle are needed to create resilient soft electronic and robotic systems.

Here, we show a liquid metal-elastomer composite as a regenerative soft electronic platform through the controlled reconfiguration of liquid metal droplet microstructure (Fig. 1a). The elastomer is a styrene-isoprene-styrene (SIS) block copolymer, which is physically cross-linked and can be reprocessed in contrast to conventional covalent networks. Together, the reconfigurable droplets and reprocessable polymer matrix enable robust, strain-invariant electrical circuitry that is self-healing, reconfigurable, and ultimately recyclable (Fig. 1b). The liquid metal droplets are initially dispersed in the matrix as electrically insulated, discrete particles that are transformed through a scalable embossing approach into connected liquid metal networks. Embossing can tune initial resistance over two orders of magnitude with initial electrical conductivities as high as 150 S cm^{-1} at 0% strain. These traces can be stretched with nearly constant resistance over numerous cycles, giving conductivities as high as $45\,400 \text{ S cm}^{-1}$ at 1200% strain. During extreme damage, the liquid metal droplets reconfigure to autonomously heal and

maintain electrical conductivity, while the tough polymer matrix allows for stretchability $>900\%$ with multiple significant damage events. As the polymer network is reprocessable, circuits can be locally reconfigured to change circuit architecture during active operation and deployment, or can be completely recycled back into dispersed and discrete liquid metal droplets over multiple cycles. We anticipate that these completely regenerative soft electronics represent a tunable platform to create resilient and recyclable circuitry for application in robotics and electronics.

Results

Elastomer-plasticizer-liquid metal system. The elastomer matrix is an SIS physically cross-linked block copolymer with an addition of polybutadiene (PBD) as a plasticizer to further tune mechanical and embossing properties. This matrix/plasticizer is specifically chosen as it displays four key characteristics, it is soft, highly deformable, tough, and can be locally or globally reprocessed with solvents to manipulate the elastomer-liquid metal microstructure to reconfigure and recycle the composite. We utilize a solution processing approach to first dissolve the solid SIS pellets in toluene and then add plasticizer as a volume ratio of SIS ($\delta = \frac{\text{PBD}}{\text{PBD}+\text{SIS}}$). This is carried out through high-shear mixing in a planetary mixer. Liquid metal is then added to this solution at a concentration of $\phi = 60\%$ liquid metal ($\phi = \frac{\text{Liquid metal}}{\text{PBD}+\text{SIS}+\text{Liquid metal}}$) and mixed to create a suspension of discrete micron-sized liquid metal droplets with diameter of $27.8 \pm 7.7 \mu\text{m}$ (Supplementary Fig. 1a–c). We have created three compositions of the liquid metal composites: (1) $\phi = 50\%$, $\delta = 0\%$; (2) $\phi = 60\%$, $\delta = 10\%$; and (3) $\phi = 60\%$, $\delta = 20\%$.

Embossing for tunable and highly stretchable conductive traces. Conductive traces are created in selected regions through a scalable embossing approach. This technique gives us the unique ability to selectively fabricate tunable, conductive traces. The as-cast SIS-PBD-liquid metal composite system contains homogeneous dispersed droplets of liquid metal. During embossing, the application of a compressive load through a stamp with prescribed positive features causes plastic deformation of the material, resulting in percolation of the liquid metal droplets into a connected network in the region of embossing (Fig. 2a). The optical micrograph of a representative embossed region in Fig. 2b shows the conductive trace left after embossing, and the surface profile can be seen in Supplementary Fig. 2a–c. This embossing technique can be utilized as a versatile and on-demand rapid approach to create intricate electrically conductive traces on a sheet of the composite through designed stamp architectures. We demonstrate this in Fig. 2c, where the letters “L” and “M” are embossed using multiple intricate conductive traces, using a positive stamp. Furthermore, the embossed conductive traces show a decreasing yet nearly constant resistance during stretching to extreme deformations, which makes them highly suitable for stretchable conductors. To characterize the electrical performance, composites are laser cut into ASTM standard dogbone samples and conductive traces are embossed along the length. The ratio of instantaneous (R) to initial (R_0) electrical resistance is measured during deformation. This normalized resistance (R/R_0) is initially equal to 1 and decreases as a strain is applied to reach a value of 0.56 before it finally breaks at a strain of 1200%. In comparison, a metallic conductor, which is stretched in a similar manner, is predicted to reach a final R/R_0 of 169 (ref. 22). The experimental curve of R/R_0 for our composite and the theoretical prediction are plotted as a function of applied strain in Fig. 2d, showing the exceptional electrical characteristics and

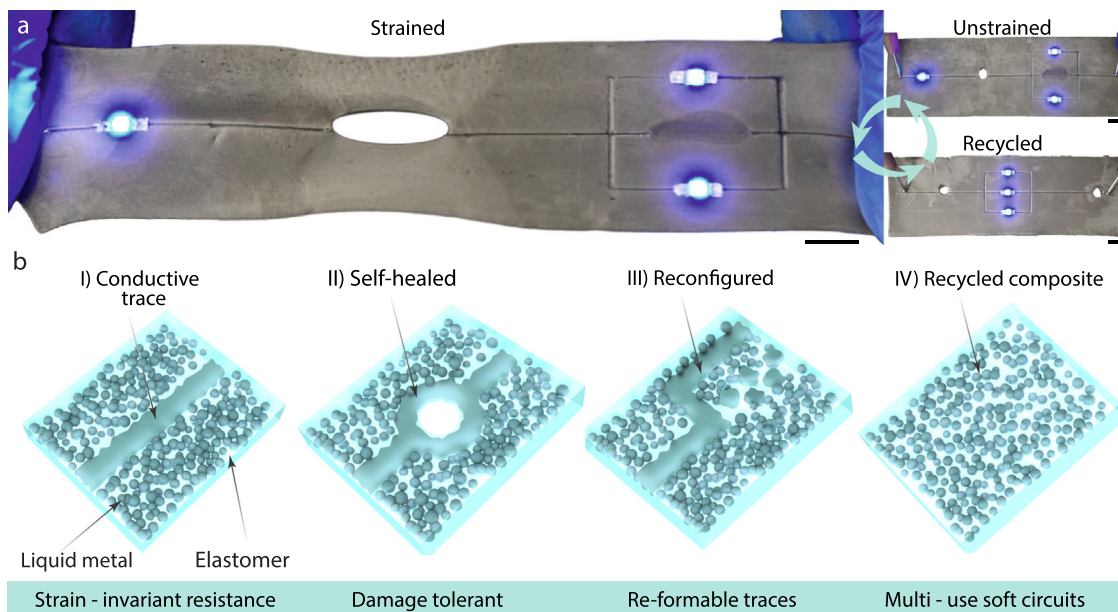


Fig. 1 Liquid metal composites for regenerative electronics. **a** A liquid metal composite demonstrated as a singular system for soft circuits with robust, self-healable conductive traces with strain-invariant resistance at different resistance levels. Unstrained and recycled samples show the LEDs functioning before stretching and after recycling (scale bars—10 mm). Material composition $\phi = 60\%$, $\delta = 20\%$. **b** Schematics show the transformation of liquid metal microstructure to enable the above capabilities—strain-invariant resistance of a conductive trace created through embossing to form a network of liquid metal particles. Damage tolerant traces through an autonomous reconfiguration of liquid metal particle connections for self-healing electronics. Reformable traces are enabled by erasing a previously formed liquid metal network and creation of a new network through a solvent erase approach. Multiuse soft circuits through dissolving the composite, which erases all liquid metal networks and electrical traces, and recycling for use in new applications.

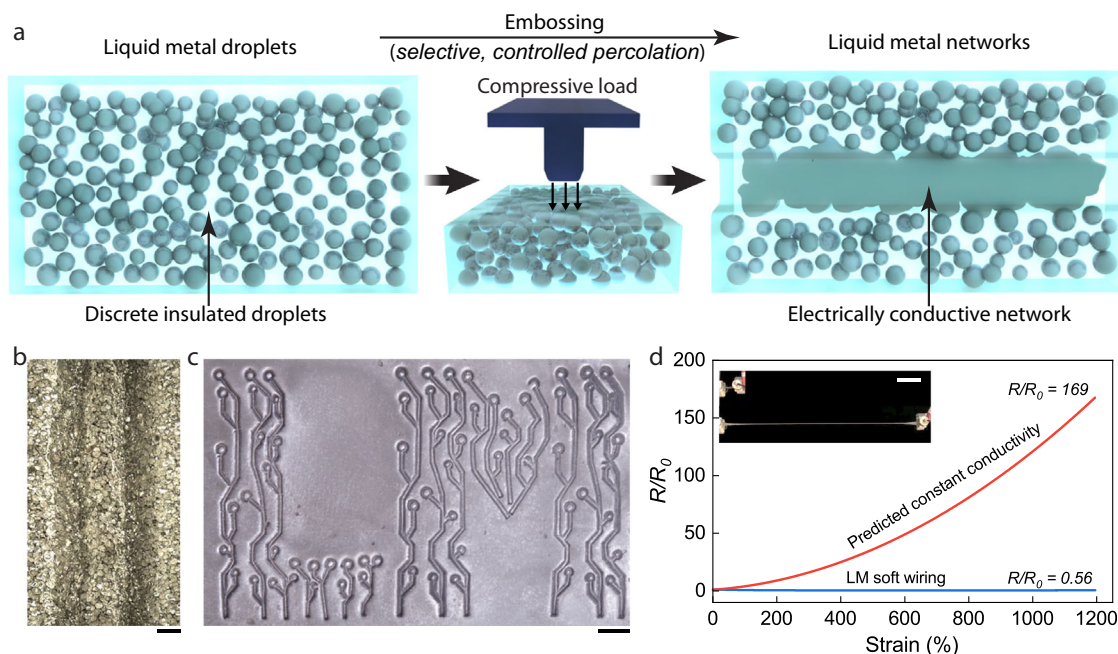


Fig. 2 Creating robust conductive traces. **a** Schematics to illustrate the process of embossing, where discrete insulating droplets of liquid metal are selectively embossed to form a connected conductive network. **b** Optical micrograph of an embossed region shows the distressed composite, which is electrically conductive, scale bar—250 μm . **c** Embossed pattern in the form of letters L and M with intricate lines and connections (scale bar—10 mm). **d** A plot of R/R_0 vs. applied strain on a conductive trace ($\phi = 60\%$, $\delta = 10\%$). The red curve shows the predicted R/R_0 increase with applied strain for a metallic conductor, while the embossed liquid metal conductive trace (blue curve) shows constant or a reduction of R/R_0 (0.56 at 1200% strain compared to 169 for the prediction). The inset shows images of an unstrained sample and a sample at 1200% strain (scale bar—50 mm).

stretchability of the embossed traces. The initial electrical conductivity can be calculated from the trace dimensions as 150 S cm^{-1} , which reaches as high as $45\,400 \text{ S cm}^{-1}$ at 1200% strain. These values of conductivity and normalized resistance at maximum strain

are exceptional compared to a wide range of previous stretchable conductors^{18,22,35–47}, highlighting the electrical performance and extreme compliance of our resilient liquid metal composite conductors (Supplementary Fig. 3a, b).

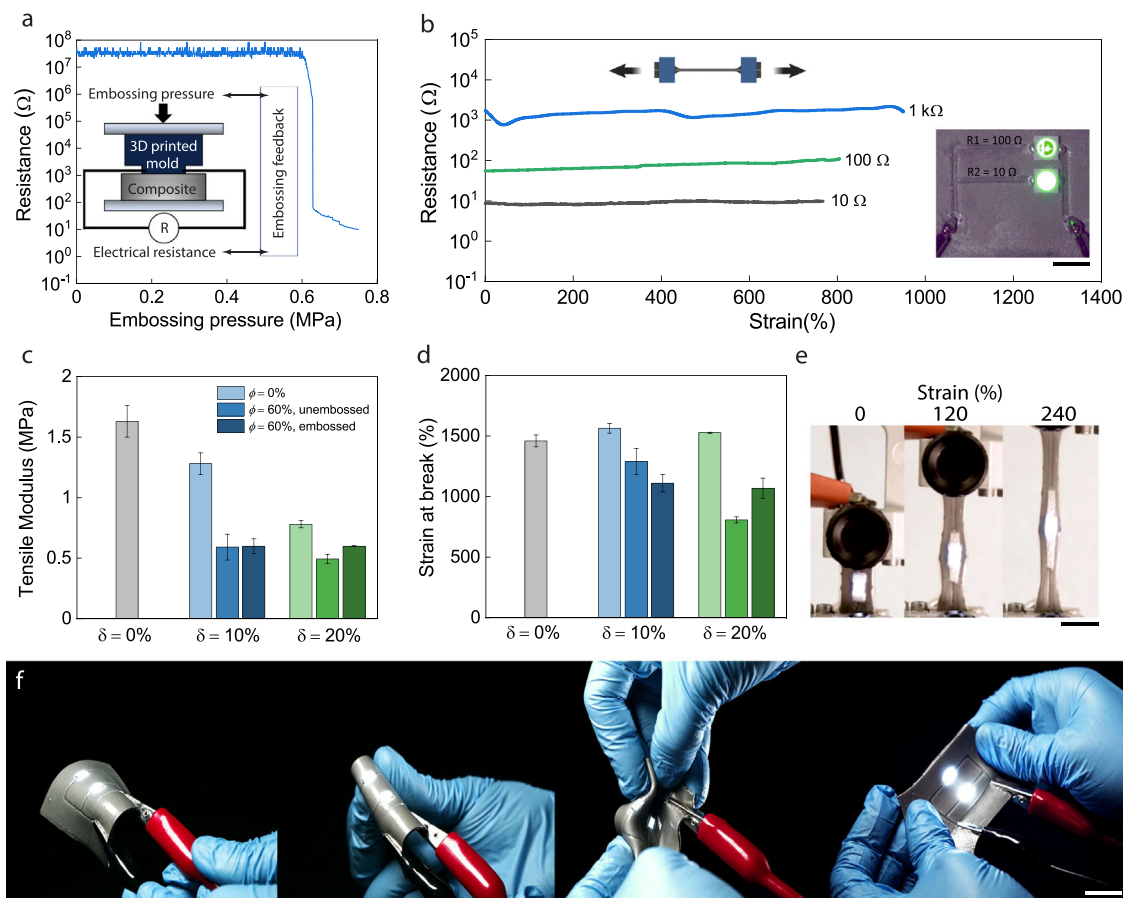


Fig. 3 Electromechanical properties of the soft conductive traces. **a** A plot and schematic illustrates the embossing procedure with feedback control. **b** A plot of resistance vs. applied tensile strain of three different conductive traces embossed to resistances $R = 10 \Omega$, 100Ω , and $1 \text{ k}\Omega$ ($\phi = 60\%$, $\delta = 20\%$). The inset shows a photograph of embossed traces with $R_1 = 100 \Omega$ and $R_2 = 10 \Omega$ being used as resistors to change LED brightness (scale bar—5 mm). **c** Tensile modulus and **d** strain at break of an unfilled elastomer, pristine (unembossed), and embossed composite. **e** Stretching of an LED integrated with embossed traces (scale bar—10 mm). **f** A composite with $\phi = 50\%$ used to create an LED circuit to illustrate the robustness of the traces in operation—bending, folding, twisting, and stretching (scale bar—10 mm). Error bars denote standard deviations for $n = 3$.

Figure 3a inset shows a schematic of the embossing setup with a representative curve of electrical resistance as a function of stress during embossing. The compressive load applied through a mechanical testing machine is controlled, while simultaneously measuring the resistance through a source meter. This synchronous setup facilitates the tuning of resistance and load applied, where either of these parameters can be used to trigger and start/stop the test. In a typical embossing step, as the load is being applied, the measured resistance remains at a high level of $\sim 10^7 \Omega$ until a threshold point, when it quickly drops and then decreases gradually with further application of load (Fig. 3a). Utilizing the designed embossing setup allows for tunable resistance based on embossing load. The applied load is increased until a target resistance is obtained, then the load is automatically stopped by sending an electronic trigger to the mechanical testing machine. This technique is used to create highly stretchable resistors in the range of 10Ω – $1 \text{ k}\Omega$ with conductivity of 190 – 0.95 S cm^{-1} , respectively, in an unstrained state. These resistors maintain a nearly constant resistance until failure at $\sim 800\%$ strain, as seen in Fig. 3b. To qualitatively demonstrate these resistors in operation, we create an LED circuit with two resistors $R_1 = 100 \Omega$ and $R_2 = 10 \Omega$ arranged in parallel. When powered, due to the difference in resistance, the LED on the lower resistor R_2 is brighter, as illustrated in Fig. 3b inset.

To determine the effect on the mechanical behavior of plasticizer on the SIS matrix and embossing on the composite

sample, we have tested pristine and embossed ASTM standard dogbones in tension (see Supplementary Fig. 4a, b). The tensile modulus and strain at break values for the composites are presented in Fig. 3c, d, respectively. We examine the unfilled elastomer and composites in the unembossed and embossed conditions for liquid metal content ($\phi = 60\%$) at two different plasticizer contents ($\delta = 10, 20\%$). Compared to an unfilled SIS elastomer, the tensile modulus decreases with the addition of the PBD plasticizer (Fig. 3c). Adding liquid metal at $\phi = 60\%$ to an SIS matrix with PBD further reduces the tensile modulus to $\sim 500 \text{ kPa}$, and the embossed sample remains similar to the unembossed sample. The strain at break for an unfilled SIS matrix shows negligible variation by the addition of PBD. When liquid metal is added to the plasticized SIS matrix, the strain at break slightly decreases but stays above 1000% strain. Taken together, these results show that the SIS matrix becomes softer by adding liquid metal droplets and plasticizer and the sample is still able to be stretched to high strains $>1000\%$, and this soft mechanical response is maintained after embossing.

The embossed composites can also interface with rigid electrical components. Here, a liquid metal contact pad is added to the end of an embossed trace where the LED is to be placed, and then is encapsulated with an unfilled SIS elastomer film (see Supplementary Fig. 5). In Fig. 3e, we present an image sequence of the LED circuit during stretching, which shows the LED functioning to $\sim 240\%$ strain (Supplementary Movie 1). As the

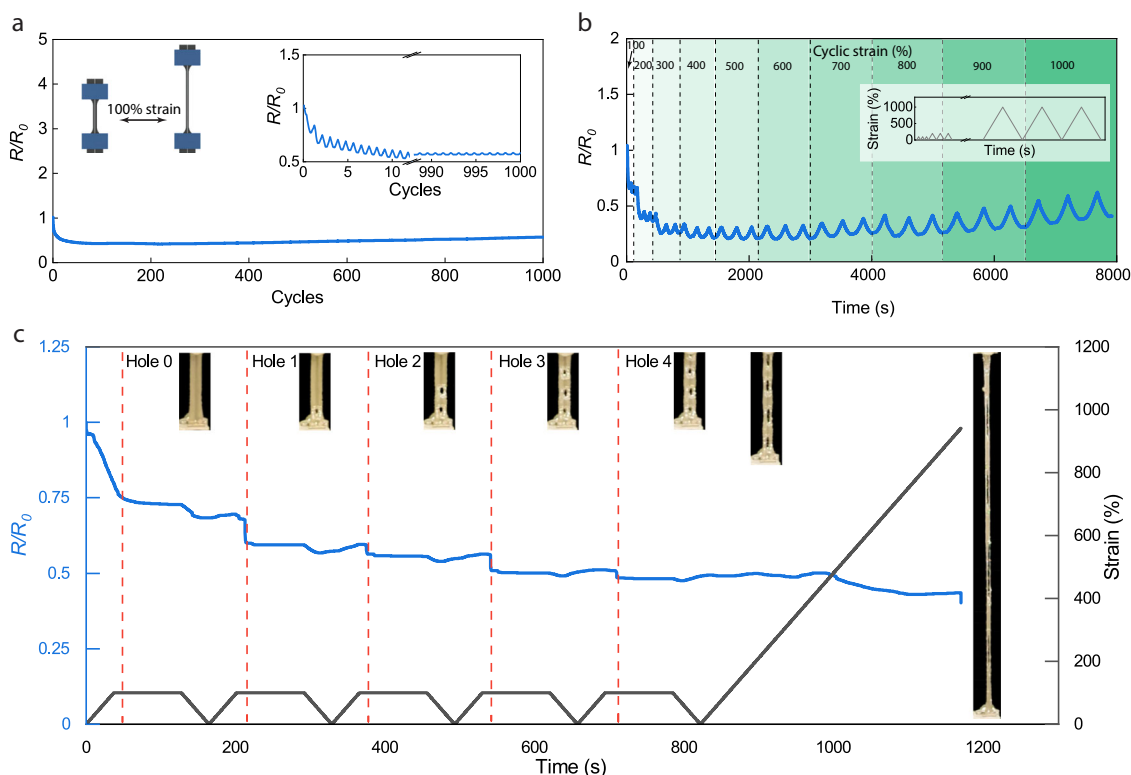


Fig. 4 Robust operation and dynamic self-healing. **a** Plot shows the robust cyclic behavior of the composite over 1000 cycles, each up to a 100% strain. **b** Plot of R/R_0 vs. time in a cyclic test of three cycles at each step up to a strain of 10000% in 100% strain increments (shading indicates the three cycles at a given strain), inset shows the applied strain profile vs. time. **c** Hole-punch test during tension shows the dynamic self-healing capability. A plot of R/R_0 with respect to strain and time shows the reduction in resistance, but shows no loss in electrical conductivity. The composition for all samples in this figure is $\phi = 60\%$, $\delta = 10\%$.

circuit fails below the high strain limits ($>10000\%$) of our conductive traces, we believe the connection failed at the LED-conductive trace interface. Images of a second circuit with two LEDs being bent, folded, twisted, and stretched in Fig. 3f further highlight the ability to integrate rigid components into our embossed conductive traces.

Control of soft electronic composite life cycle. We demonstrate our embossed liquid metal composites as regenerative electronics as introduced in Fig. 1 through (1) robust operation, (2) self-healing, (3) circuit reconfiguration, and (4) recycling for full life cycle control. Broadly, the first three phases can occur during the life of the composite, while the recycling phase is at the end of life when the composite utility is exhausted and needs to be regenerated/refurbished to create a new composite sheet with almost pristine properties.

Robust operation. To understand the properties of the embossed conductive traces in repetitive operation, we perform cyclic tests in tension. We utilize an embossed trace on a composite with $\phi = 60\%$ liquid metal and $\delta = 10\%$ PBD to strain up to 100% for 1000 cycles (Fig. 4a, the first and last ten cycles in the inset). Figure 4b shows another cyclic test up to higher strains, where a sample with same composition is subjected to a maximum strain of 10000% in 100% strain increments with three cycles at each increment (each cycle returns to 0% strain). Both tests demonstrate the exceptional electromechanical behavior of the traces. Overall, the resistance change is very low or actually decreases during stretching as shown by the R/R_0 equal to or <1 during all of the cyclic tests. This behavior is unexpected for a bulk metallic conductor. For example, in a typical conductive wire, the R/R_0

ratio can be predicted by using the stretch ratio as $R/R_0 = \lambda^2$ (where $\lambda = \text{strain} + 1$)⁴⁸. At a strain of 100% ($\lambda = 2$), the predicted $R/R_0 = 4$, and similarly when the wire is stretched to 10000% strain ($\lambda = 11$), the predicted ratio $R/R_0 = 121$. During the 100% strain cyclic experiment for our embossed traces, the (R/R_0) = 1 at 0% strain and then nominally drops to $R/R_0 \sim 0.6$ with a peak to valley change in $R/R_0 \sim 0.001$ near the 1000th cycle. During the incremental increasing strain cycling, we observe a similar behavior, where even during the final cycles at 10000%, $R/R_0 \sim 0.6$ with a peak to valley change in $R/R_0 \sim 0.20$. These results highlight our embossed conductive traces as promising candidates for soft circuit wiring at extreme strain levels over multiple cycles.

Self-healing. As highlighted in the introduction, self-healing ability is a critical property for soft materials in rugged environments. We demonstrate this self-healing and mechanical robustness by punching four consecutive holes into an actively stretched embossed composite, which maintains conductivity during the whole damage process and is able to be stretched to $\sim 950\%$ strain (Supplementary Movie 2). These holes remove sections of the composite material along the embossed trace during a six-step process. In the first step, the dogbone is stretched to 100% strain, rested for 45 s, and brought back to 0% strain. In the second step, a hole (damage event 1) is punched during the resting period at 100% strain. The third, fourth, and fifth steps result in three more holes on the embossed trace. In the sixth step, the dogbone is stretched from 0% strain until it fails. The visual appearance of the dogbone is continuously monitored and images at important stages are presented adjacent to the event in Fig. 4c. The applied strain and the ratio of instantaneous

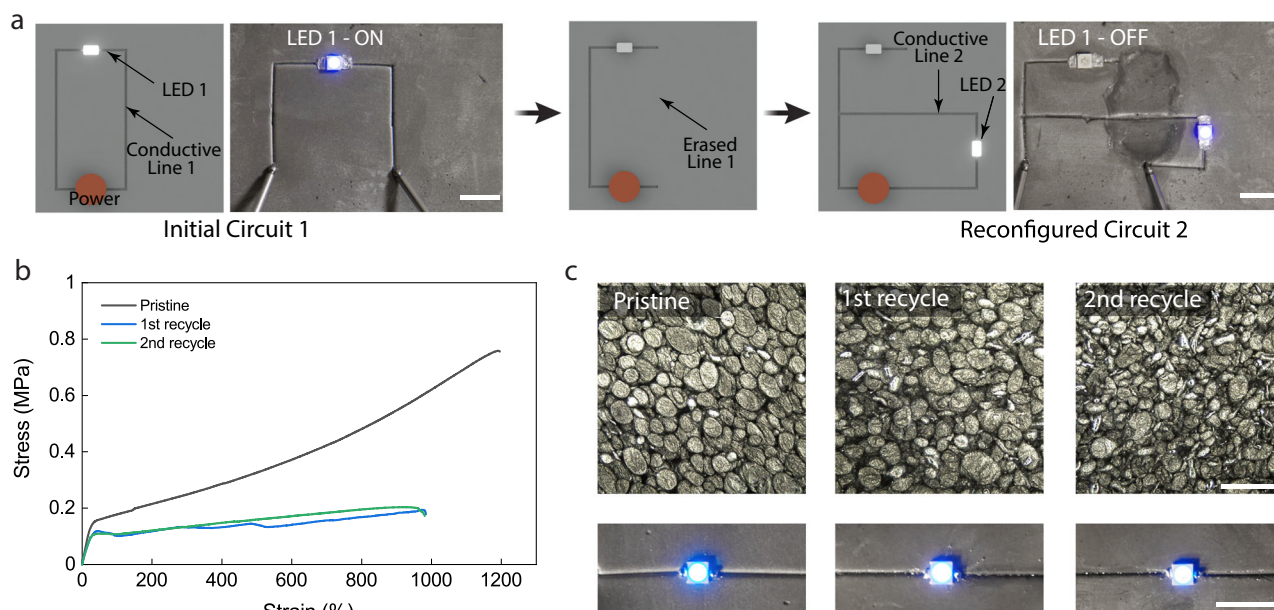


Fig. 5 Reconfiguration and recycling of liquid metal soft composite. **a** Schematics and photographs showing the reconfiguration process of a conductive trace by solvent erase approach in a composite with $\phi = 60\%$, $\delta = 20\%$, scale bars—10 mm. **b** Stress–strain curves of the pristine, and recycled samples showing a higher stress level for the pristine. **c** Optical micrographs show the change in liquid metal droplet microstructure with recycling and the LEDs show no loss of electrical functionality in a composite with $\phi = 60\%$, $\delta = 10\%$ (scale bar for micrographs—100 μm and images—10 mm).

to initial electrical resistance (R/R_0) with respect to time are plotted in Fig. 4c. The ratio (R/R_0) drops as stretching begins and slightly reduces at each damage event. There is no loss of electrical functionality at any stage during the test even with significant portions of the composite being removed along the embossed line. This is due to the instant self-healing ability of the liquid metal network, which autonomously reconfigures to form new liquid metal particle–particle connections around a damaged site. These new networks form during the damaging process and thus maintain continuous electrical conductivity. While self-healing in a liquid metal composite has been demonstrated in previous research³⁰, it has been limited to an unstrained condition. With an ability to instantly self-heal to maintain electrical conductivity and also be mechanically tough to sustain significant and critical damage events under strain, our material combination enables mechanically and electrically robust stretchable conductors.

Circuit reconfiguration. The ability of the SIS polymer to dissolve in toluene enables an embossed trace to be locally erased and then form a new conductive trace through the same region to reconfigure the circuit. This process occurs as the solvent locally separates the liquid metal network during the treatment to effectively erase that specific region of the trace. In Fig. 5a, a schematic for reconfiguration procedure along with the images of initial and reconfigured circuits are presented. Initially, LED 1 is connected to a power source through two traces on each side and the LED lights up when a current is applied. In the second step, one of the traces is erased partially using the toluene solvent, thus resulting in an open circuit which turns off the LED 1. In the third step, two new traces (one through the erased region) are created and a second LED (LED 2) is placed on the composite sheet. Now with the application of current, the LED 2 lights up and LED 1 remains turned off. This demonstrates an important ability in our composite system to reconfigure circuit elements in a nondestructive manner.

Recycling. The thermoplastic nature of the SIS copolymer matrix coupled with the liquid nature of liquid metal enables us to

effectively recycle and reuse the composites. We demonstrate this through a solution process, where the used composite sheets at the end of their life are rapidly dissolved by toluene in a shear mixer. This results in a SIS, PBD, and toluene solution with dispersed liquid metal droplets similar to the initial pristine composite. This emulsion can then be cast into films using the same conditions as the pristine composite. In Fig. 5b, we show the mechanical behavior of an as-made pristine composite ($\phi = 60\%$, $\delta = 10\%$) and after being recycled twice. The initial stiffness of the pristine and recycled composites are similar. At higher strain, the stress–strain behavior of the pristine composite shows a more significant strain stiffening response than the recycled samples. However, both the recycled samples reach $\sim 1000\%$ strain, which indicates robust properties of the reprocessed composite. The microstructure of the liquid metal droplets in the composite generally maintain the spherical/ellipsoidal shape even after the second recycle cycle (Fig. 5c). The recycled samples are electrically insulating after casting, demonstrating that all of the previous electrical connections have been erased. This indicates that the previous liquid metal networks get completely broken down back into liquid metal droplets. These recycled composites can then again be embossed to create electrical circuitry. We demonstrate this capability by creating functional LED circuits on the pristine and two generations of recycled samples (Fig. 5c). We apply current for 1, 3, and 5 s with 1 s intervals which indicates the reliability of the electrical connections in the pristine and the recycled samples (Supplementary Movie 3).

Discussion

Rehealable and recyclable soft electronics that can be stretched to high strains ($>1000\%$) can provide robust solutions for emerging fields like soft and stretchable electronics and soft robotics. This is especially relevant for soft functional materials, which can be vulnerable, as they cannot be protected with stiff external supports and enclosures like rigid electronics. In this work, we have shown a single multifunctional composite system for soft electronics that shows robust stretchability, rehealing ability, and is ultimately

recyclable. Although we have demonstrated this approach with micron-sized (~30 μm) liquid metal droplets, it may be possible to further tune mechanical and electrical properties by changing the particle size. A systematic study on the size effects could extend the applicability of our design to further control initial trace resistance, tune the embossing process through different resistance-embossing pressure profiles, control the degree of undercooling, or improve breakdown voltage^{25,49–51}. This size limitation could be overcome by utilizing techniques, such as sonication to create submicron liquid metal droplets, which would still allow us to process our materials as emulsions³². Further long-term testing could also provide information on the longevity and fatigue characteristics of the different generations of recycled soft materials.

In conclusion, our soft composite approach utilizes the unique ability of liquid phase inclusions to reconfigure their microstructure to make, maintain, and break robust liquid metal networks for full life cycle control in soft electronics. When coupled with the reprocessing of the physically cross-linked elastomer matrix, we gain the ability to process the liquid metal microstructure for network formation, and subsequently reconfigure or regenerate to the pristine microstructure by either local or bulk reprocessing. This control of liquid metal microstructures within the composite imparts the essential electrical functions for resilient and regenerative soft electronics. The embossing creates connections that can reconfigure during damage. Reprocessing the matrix can then break these connections locally to reconfigure circuits or globally to break down all liquid metal networks to restore the material back to the original electrically insulating state with discrete liquid metal droplets. This material can then be reprocessed to create new soft, liquid metal electronics. These properties improve resilience in soft devices, which can be utilized for diverse functionalities in soft electronics and robotics. Such capabilities can further enable robust soft electronics that can reduce electronic waste through improved lifetime and recyclability.

Methods

Composite fabrication. The liquid metal composites are fabricated by casting a solution of SIS block copolymer, liquid metal (EGaIn), PBD, and toluene. Liquid metal is a eutectic alloy of gallium and indium in 3:1 ratio, which is combined at room temperature and homogenized at 200 °C overnight on a hot plate. First, the as-obtained SIS pellets from Sigma Aldrich are dissolved in toluene in a dual asymmetric centrifugal mixer (FlackTek Speedmixer) followed by addition of PBD. To this solution, a calculated amount of liquid metal is added and mixed in the centrifugal mixer, which breaks down the liquid metal filler into smaller droplets and forms a homogeneous suspension. The cast sheets solidify at room temperature for 24 h in a fume hood to allow for the removal of toluene and then at an elevated temperature of 80 °C in a convection oven for 24 h. The typical thickness of a composite sheet is 1.5 mm.

Recycling. We solution process the used composite sheets at the end of their life through a two-step dissolution process, using a shear mixer. In the first step, a calculated $\left(\sigma = \frac{\text{Toluene}}{\text{SIS} + \text{PBD} + \text{Toluene}}\right)$ amount of toluene solvent is added to ~1 cm × 1 cm cut pieces of the composite sheet. In the second step, the pieces with the solvent are shear mixed in a planetary mixer for 6 min at 2000 r.p.m. Films are then cast as described above.

Electromechanical testing

Compression test/embossing. This describes the procedure used to create the conductive traces/wiring. A 3D printed mold (B9 Creator v1.2) with a line feature (thickness ~1 mm) is placed on top of the sample (see Fig. 3a) in a compression test setup on an Instron 5944 mechanical testing machine. Conductive tape is attached at the ends of this line and connected to a Keithley 2460 source measuring unit (SMU) to send a constant current of 100 mA and measure the voltage during compression. Both these instruments are synchronized and when a desired load/resistance is reached, triggers are sent to the mechanical/electrical measurement programs to stop the measurement simultaneously. MATLAB software is utilized to control and export data from the SMU.

Tension test. For tension testing, the composite sheet is cut into a dogbone shape using a CO₂ laser cutter (Epilog). The dogbone is set to be 50% of ASTM D412 C-type standard size. A 3D printed mold with a line feature of thickness 1 mm and length equal to the dogbone length (57.5 mm) is used to emboss the conductive trace. Both unembossed and embossed dogbone samples are tested in uniaxial tension. The tensile modulus is calculated with a linear fit up to 5% strain. For cyclic testing, the same ASTM dogbone geometry and embossing process is used. A Keithley SMU measures resistance outside the test grips.

Micrography. Optical microscopy is performed on a Leica DMi8 inverted microscope in dark-field mode. To construct a 3D profile of the embossed line, multiple images are taken in the region of interest and stacked along z-axis (through thickness). The 3D profile gives important parameters of the feature, such as depth of embossed line relative to the surface and how this varies through the sample thickness.

Soft circuit fabrication. To create a soft circuit, conductive traces are made on a liquid metal–elastomer–plasticizer composite sheet at predetermined locations, using 3D printed molds. Liquid metal paste (liquid metal + 7 vol% Cu microparticles) is stencil printed at the interfaces of the component ends. This liquid metal + Cu microparticle ratio is chosen as it creates a semisolid mixture⁵², which maintains good electrical contact without flowing. Electronic components, such as LEDs, are then glued at desired points and connected to the traces with liquid metal paste. This composite sheet with electronic components and conductive traces is encapsulated by a 200 μm thin SIS layer at 150 °C and 25 mbar vacuum. This process flow is schematically outlined in Supplementary Fig. 5.

Data availability

The data that support the findings of this study are available from the corresponding author upon reasonable request.

Received: 8 March 2021; Accepted: 19 May 2021;

Published online: 14 June 2021

References

- Polygerinos, P., Wang, Z., Galloway, K. C., Wood, R. J. & Walsh, C. J. Soft robotic glove for combined assistance and at-home rehabilitation. *Robot. Auton. Syst.* **73**, 135–143 (2015).
- Rogers, J., Malliaras, G. & Someya, T. Biomedical devices go wild. *Sci. Adv.* **4**, eaav1889 (2018).
- Lin, S. et al. Stretchable hydrogel electronics and devices. *Adv. Mater.* **28**, 4497–4505 (2016).
- Yu, Y. et al. Multifunctional “hydrogel skins” on diverse polymers with arbitrary shapes. *Adv. Mater.* **31**, 1807101 (2019).
- Bartlett, M. D., Dickey, M. D. & Majidi, C. Self-healing materials for soft-matter machines and electronics. *NPG Asia Mater.* **11**, 1–4 (2019).
- Baran, D., Corzo, D. & Blazquez, G. T. Flexible electronics: status, challenges and opportunities. *Front. Electron.* **1**, 2 (2020).
- Patrick, J. F., Robb, M. J., Sottos, N. R., Moore, J. S. & White, S. R. Polymers with autonomous life-cycle control. *Nature* **540**, 363–370 (2016).
- White, S. R. et al. Autonomic healing of polymer composites. *Nature* **409**, 794–797 (2001).
- Markvicka, E. J., Tutika, R., Bartlett, M. D. & Majidi, C. Soft electronic skin for multi-site damage detection and localization. *Adv. Funct. Mater.* **29**, 1900160 (2019).
- Feig, V. R., Tran, H. & Bao, Z. Biodegradable polymeric materials in degradable electronic devices. *ACS Central Sci.* **4**, 337–348 (2018).
- Mazzolai, B. & Laschi, C. A vision for future bioinspired and biohybrid robots. *Sci. Robot.* **5**, eaab6893 (2020).
- Kang, J., Tok, J. B.-H. & Bao, Z. Self-healing soft electronics. *Nat. Electron.* **2**, 144–150 (2019).
- Bauer, S. et al. 25th anniversary article: a soft future: from robots and sensor skin to energy harvesters. *Adv. Mater.* **26**, 149–162 (2014).
- Hwang, S.-W. et al. High-performance biodegradable/transient electronics on biodegradable polymers. *Adv. Mater.* **26**, 3905–3911 (2014).
- Yin, L. et al. Dissolvable metals for transient electronics. *Adv. Funct. Mater.* **24**, 645–658 (2014).
- Hwang, S.-W. et al. Biodegradable elastomers and silicon nanomembranes/nanoribbons for stretchable, transient electronics, and biosensors. *Nano Lett.* **15**, 2801–2808 (2015).
- Qiu, S. et al. Mechanically and electrically robust stretchable e-textiles by controlling the permeation depth of silver-based conductive inks. *Flex. Print. Electron.* **4**, 025006 (2019).

18. Vural, M., Behrens, A. M., Ayyub, O. B., Ayoub, J. J. & Kofinas, P. Sprayable elastic conductors based on block copolymer silver nanoparticle composites. *ACS Nano* **9**, 336–344 (2015).
19. Zou, Z. et al. Rehealable, fully recyclable, and malleable electronic skin enabled by dynamic covalent thermoset nanocomposite. *Sci. Adv.* **4**, eaaq0508 (2018).
20. Style, R. W., Tutika, R., Kim, J. Y. & Bartlett, M. D. Solid-liquid composites for soft multifunctional materials. *Adv. Funct. Mater.* **31**, 2005804 (2021).
21. Dickey, M. D. Stretchable and soft electronics using liquid metals. *Adv. Mater.* **29**, 1606425 (2017).
22. Thrasher, C. J., Farrell, Z. J., Morris, N. J., Willey, C. L. & Tabor, C. E. Mechanoresponsive polymerized liquid metal networks. *Adv. Mater.* **31**, 1903864 (2019).
23. Haque, A. T., Tutika, R., Byrum, R. L. & Bartlett, M. D. Programmable liquid metal microstructures for multifunctional soft thermal composites. *Adv. Funct. Mater.* **30**, 2000832 (2020).
24. Wang, H. et al. A highly stretchable liquid metal polymer as reversible transitional insulator and conductor. *Adv. Mater.* **31**, 1901337 (2019).
25. Ralphs, M. I. et al. In situ alloying of thermally conductive polymer composites by combining liquid and solid metal microadditives. *ACS Appl. Mater. Interfaces* **10**, 2083–2092 (2018).
26. Hirsch, A., Michaud, H. O., Gerratt, A. P., De Mulatier, S. & Lacour, S. P. Intrinsically stretchable biphasic (solid-liquid) thin metal films. *Adv. Mater.* **28**, 4507–4512 (2016).
27. Palleau, E., Reece, S., Desai, S. C., Smith, M. E. & Dickey, M. D. Self-healing stretchable wires for reconfigurable circuit wiring and 3d microfluidics. *Adv. Mater.* **25**, 1589–1592 (2013).
28. Teng, L. et al. Liquid metal-based transient circuits for flexible and recyclable electronics. *Adv. Funct. Mater.* **29**, 1808739 (2019).
29. Chang, H. et al. Direct writing and repairable paper flexible electronics using nickel-liquid metal ink. *Adv. Mater. Interfaces* **5**, 1800571 (2018).
30. Markvicka, E. J., Bartlett, M. D., Huang, X. & Majidi, C. An autonomously electrically self-healing liquid metal-elastomer composite for robust soft-matter robotics and electronics. *Nat. Mater.* **17**, 618–624 (2018).
31. Blaiszik, B. J. et al. Autonomic restoration of electrical conductivity. *Adv. Mater.* **24**, 398–401 (2012).
32. Boley, J. W., White, E. L. & Kramer, R. K. Mechanically sintered gallium-indium nanoparticles. *Adv. Mater.* **27**, 2355–2360 (2015).
33. Liu, S. et al. Laser sintering of liquid metal nanoparticles for scalable manufacturing of soft and flexible electronics. *ACS Appl. Mater. Interfaces* **10**, 28232–28241 (2018).
34. Ford, M. J., Patel, D. K., Pan, C., Bergbreiter, S. & Majidi, C. Controlled assembly of liquid metal inclusions as a general approach for multifunctional composites. *Adv. Mater.* **32**, 2002929 (2020).
35. Lipomi, D. J. et al. Skin-like pressure and strain sensors based on transparent elastic films of carbon nanotubes. *Nat. Nanotechnol.* **6**, 788–792 (2011).
36. Liang, J., Tong, K. & Pei, Q. A water-based silver-nanowire screen-print ink for the fabrication of stretchable conductors and wearable thin-film transistors. *Adv. Mater.* **28**, 5986–5996 (2016).
37. Zhu, S. et al. Ultrastretchable fibers with metallic conductivity using a liquid metal alloy core. *Adv. Funct. Mater.* **23**, 2308–2314 (2013).
38. Jiang, S. et al. Highly stretchable conductive fibers from few-walled carbon nanotubes coated on poly (m-phenylene isophthalamide) polymer core/shell structures. *ACS Nano* **9**, 10252–10257 (2015).
39. Ma, R., Kang, B., Cho, S., Choi, M. & Baik, S. Extraordinarily high conductivity of stretchable fibers of polyurethane and silver nanoflowers. *ACS Nano* **9**, 10876–10886 (2015).
40. Wang, J. et al. Printable superelastic conductors with extreme stretchability and robust cycling endurance enabled by liquid-metal particles. *Adv. Mater.* **30**, 1706157 (2018).
41. Park, M. et al. Highly stretchable electric circuits from a composite material of silver nanoparticles and elastomeric fibres. *Nat. Nanotechnol.* **7**, 803–809 (2012).
42. Matsuhisa, N. et al. Printable elastic conductors by in situ formation of silver nanoparticles from silver flakes. *Nat. Mater.* **16**, 834–840 (2017).
43. Chun, K.-Y. et al. Highly conductive, printable and stretchable composite films of carbon nanotubes and silver. *Nat. Nanotechnol.* **5**, 853–857 (2010).
44. Stoyanov, H., Kolloosche, M., Risse, S., Waché, R. & Kofod, G. Soft conductive elastomer materials for stretchable electronics and voltage controlled artificial muscles. *Adv. Mater.* **25**, 578–583 (2013).
45. Matsuhisa, N. et al. Printable elastic conductors with a high conductivity for electronic textile applications. *Nat. Commun.* **6**, 1–11 (2015).
46. Wang, Y. et al. A highly stretchable, transparent, and conductive polymer. *Sci. Adv.* **3**, e1602076 (2017).
47. Sekitani, T. et al. Stretchable active-matrix organic light-emitting diode display using printable elastic conductors. *Nat. Mater.* **8**, 494–499 (2009).
48. Keplinger, C. et al. Stretchable, transparent, ionic conductors. *Science* **341**, 984–987 (2013).
49. Pan, C. et al. A liquid-metal-elastomer nanocomposite for stretchable dielectric materials. *Adv. Mater.* **31**, 1900663 (2019).
50. Tutika, R., Kmiec, S., Haque, A. T., Martin, S. W. & Bartlett, M. D. Liquid metal-elastomer soft composites with independently controllable and highly tunable droplet size and volume loading. *ACS Appl. Mater. Interfaces* **11**, 17873–17883 (2019).
51. Martin, A., Chang, B. S., Pauls, A. M., Du, C. & Thuo, M. Stabilization of undercooled metals via passivating oxide layers. *Angew. Chem. Int. Ed.* **60**, 5928–5935 (2021).
52. Tutika, R., Zhou, S. H., Napolitano, R. E. & Bartlett, M. D. Mechanical and functional tradeoffs in multiphase liquid metal, solid particle soft composites. *Adv. Funct. Mater.* **28**, 1804336 (2018).

Acknowledgements

The authors acknowledge support through Defense Advanced Research Projects Agency Young Faculty Award (DARPA YFA; D18AP00041) and Virginia Tech. The authors would like to thank J. Mills and L. Granadillo for their assistance in sample fabrication.

Author contributions

R.T. performed experiments. R.T. and A.B.M.T.H. analyzed experimental data under the supervision of M.D.B. All authors contributed to writing and discussing the manuscript.

Competing interests

The authors declare no competing interests.

Additional information

Supplementary information The online version contains supplementary material available at <https://doi.org/10.1038/s43246-021-00169-4>.

Correspondence and requests for materials should be addressed to M.D.B.

Peer review information *Communications Materials* thanks the anonymous reviewers for their contribution to the peer review of this work. Primary Handling Editors: Jie Xu and John Plummer.

Reprints and permission information is available at <http://www.nature.com/reprints>

Publisher's note Springer Nature remains neutral with regard to jurisdictional claims in published maps and institutional affiliations.



Open Access This article is licensed under a Creative Commons Attribution 4.0 International License, which permits use, sharing, adaptation, distribution and reproduction in any medium or format, as long as you give appropriate credit to the original author(s) and the source, provide a link to the Creative Commons license, and indicate if changes were made. The images or other third party material in this article are included in the article's Creative Commons license, unless indicated otherwise in a credit line to the material. If material is not included in the article's Creative Commons license and your intended use is not permitted by statutory regulation or exceeds the permitted use, you will need to obtain permission directly from the copyright holder. To view a copy of this license, visit <http://creativecommons.org/licenses/by/4.0/>.

© The Author(s) 2021